Phases in two dimensional $p_x + ip_y$ superconducting systems with next-nearest-neighbor interactions

Antonio Russo and Sudip Chakravarty

Department of Physics and Astronomy, University of California at Los Angeles, Los Angeles, California 90095-1547, USA

A chiral $p_x + ip_y$ superconductor on a square lattice with nearest and next-nearest hopping and pairing terms is considered. Gap closures, as various parameters of the system are varied, are found analytically and used to identify the topological phases. The phases are characterized by Chern numbers (ranging from -3 to 3), and (numerically) by response to introduction of weak disorder, edges, and magnetic fields in an extreme type-II limit, focusing on the low-energy modes (which presumably become zero-energy Majorana modes for large lattices and separations). Several phases are found, including a phase with Chern number 3 that cannot be thought of in terms of a single range of interaction, and a phase with Chern number 2 that may host an additional, disorder-resistant Majorana mode. The energies of the vortex quasiparticle modes were found to oscillate as vortex position varied. The spatial length scale of these oscillations was found for various points in the Chern number 3 phase which increased as criticality was approached.

PACS number(s): 71.10.Pm, 74.90.+n, 03.67.Lx, 74.20.Rp

I. INTRODUCTION

Recently, there has been much interest in topological features of various condensed matter systems, in particular Majorana fermions.[1–15] Majorana fermions satisfy $\gamma^\dagger = \gamma$; that is, they are their own antiparticle. In systems with particle-hole symmetry, their energy is therefore pinned to zero. Consequently, Majoranas can only be destroyed by pairing with another and hybridizing into a Dirac fermion.

We focus on chiral $p_x + ip_y$ superconductors. In continuum models with nonzero Chern numbers, zero-energy Majoranas develop around defects, such as vortices.[12–19] When the vortices are well separated, the associated Majoranas are protected from local perturbations, which could be useful in quantum computers. Majoranas are also expected in lattice models of chiral superconductors; if the gap is of the form $\sin(nk_x) + i\sin(nk_y)$, where n is the range of the interaction, it reduces to $n\partial_x + in\partial_y$ in the continuum limit.

In contrast to the continuum case where the range of the interaction, n, simply rescales the gap function, the range plays a more interesting role on the lattice. Previous work[20] suggested that the inclusion of longer ranged interactions leads to novel phases. These longer ranged interactions in general give rise to larger Chern numbers in a way that can be most easily understood when all interactions are of the same range. When all interactions are of the same range, a number of nonnteracting sublattices, $S(n)$, form. For example, in Fig. 1, two sublattices form when only next-nearest-neighbor terms are present. As separate systems, each sublattice has its own Chern number, either 0 or 1. Therefore, the Chern number for the whole system is either 0 or $S(n)$.

To explore the more complicated case of interactions of different ranges, we study a square lattice with a combination of nearest-neighbor (NN) and next-nearest-neighbor (NNN) hopping (respectively, t_1 and t_2), and $p_x + ip_y$ pairing (respectively, Δ_1 and Δ_2) terms. The system is kept at chemical potential μ. Both the hopping and pairing terms are illustrated in Fig. 2.

The five parameters t_1, t_2, Δ_1, Δ_2, and μ constitute a parameter space rich enough to include the well-known BEC

and BCS superconducting systems, as well as their two-sublattice versions (i.e., purely NNN interactions). Because the BEC-BCS transition is topological in nature, we search for the surfaces in parameter space where the bulk band gap collapses and topological phase transitions occur.

Our analysis of the system shows that the phase diagram depends only on *three* ratios of parameters: $\alpha = \frac{\Delta_1}{\Delta_2}$ and the scaled hopping terms t_1/μ, t_2/μ. For fixed values of α, all phase transitions are lines in the t_1-t_2 plane. There are four such lines, three of which are independent of α. When a system is tuned to one of these phase transition lines, the gap in the system collapses because a zero of $\Delta(\mathbf{k})$ is crossing the Fermi surface. The lines constitute the phase diagram for a given value of α, as shown in Fig. 3. When $|\alpha|^2 \geqslant 2$, the phase transition lines remain fixed, and $\Delta(\mathbf{k})$ only has zeros at the four high-symmetry points Γ, X, Y, and M because the NNN pairing terms are not strong enough to introduce any zeros into $\Delta(\mathbf{k})$. The topology of the system is unaffected by the weak NNN pairing. When $|\alpha|^2 < 2$, four additional zeros are introduced into $\Delta(\mathbf{k})$, permitting larger Chern numbers. An analytical calculation finds all Chern numbers possible with NN and NNN terms; they range from -3 to $+3$. Chern number ± 4, while conceivably possible with NNN pairing terms, cannot be obtained with just NNN hopping terms for the same reason that Chern number 2 cannot be obtained with just NN pairing and hopping terms. However, the system does take on Chern number 3, which is surprising because purely NNN interactions yield Chern number 2.

The numerical aspect of the present work characterizes the response of the model system to defects in different phases. In particular, we focus on characterizing the low-energy response, i.e., identifying the the fundamental excitations of the system. For the numerics, we include three kinds of position-dependent terms into the Hamiltonian: edges, on-site disorder, and magnetic fields in an extreme type-II limit with vortices in the superconducting order parameter. Edges are introduced by adding terms of the form $O_i c_i^\dagger c_i$, where O_i is very large past the edge, confining the states in the low-energy spectrum. On-site disorder is added in a similar manner: O_i takes on a value
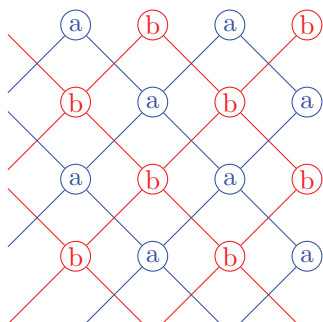
FIG. 1. (Color online) When only next-nearest-neighbor inter-actions are present in a 2 dimensional lattice model, two sublattices form, each independently responding to defects, giving pairs of defect modes. When nearest-neighbor interactions are turned on, the pairs of defect modes persist.

of E_d with probability $\frac{p}{2}$ and $-E_d$ with the same probability, and 0 otherwise. For the magnetic field, we assume a very long magnetic screening length so that the magnetic field is constant, consistent with the sample being two dimensional. However, the superconducting coherence length ξ is finite, and vortices appear in the superconducting order parameter.

The output of numerical simulations are the energies and wave functions of the quasiparticles of the Hamiltonian. The edge modes and vortex core modes are perfectly distinct in the ideal limit of infinite separation. In the realistic case of finite separation, the modes hybridize. The vortex core modes interact with each other in a similar way. The energies of the lowest vortex core modes exhibit exponentially damped oscillations as the vortices are separated, an effect theoretically predicted[21] and numerically observed[22] in related systems. The edges hybridize with vortices over longer length scale than those over which the vortices hybridize with each other.
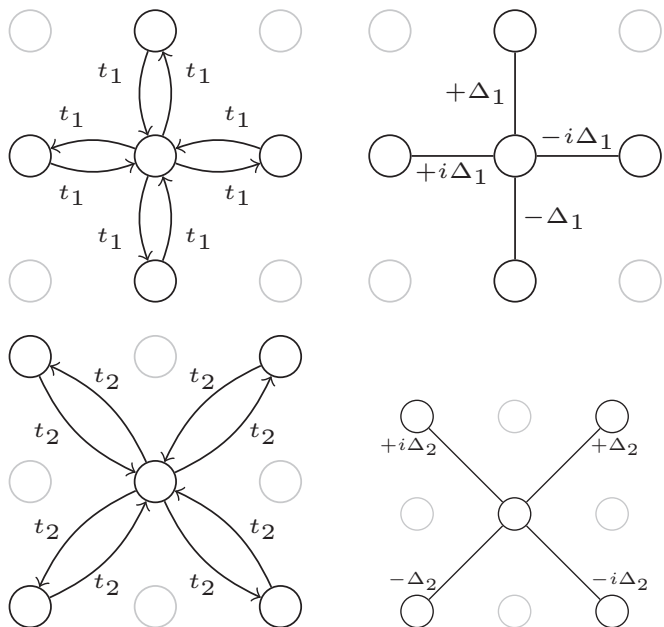

FIG. 2. Visualization of nearest- (and second-nearest-) neighbor hopping (t) and pairing (Δ) terms.
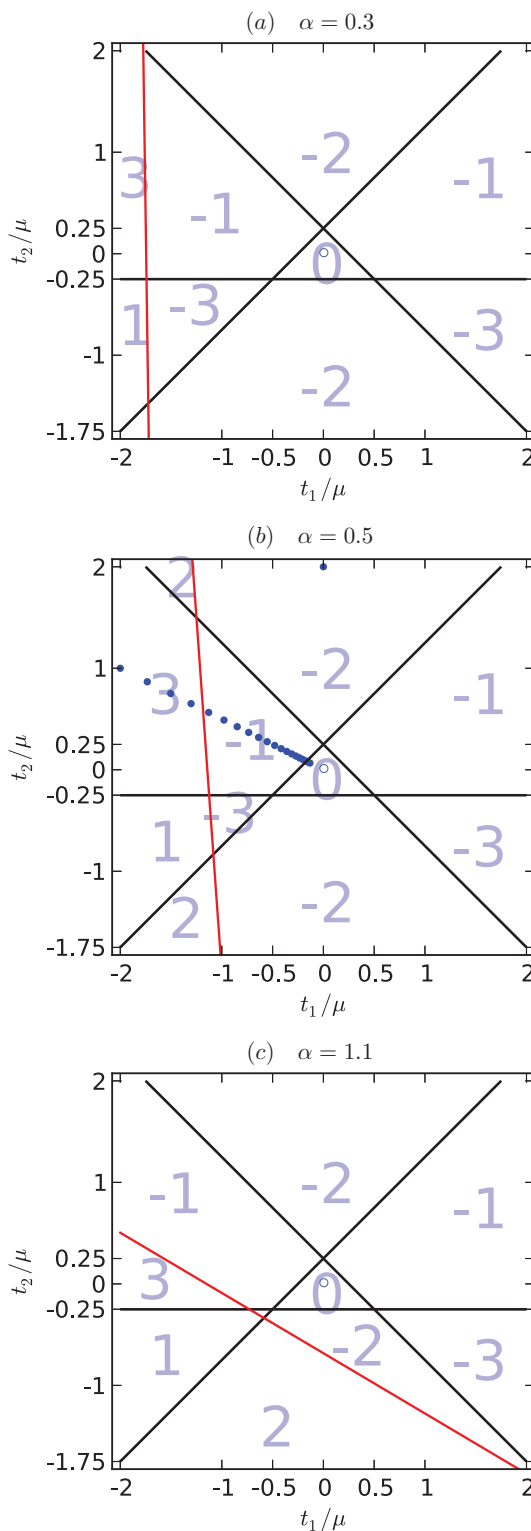

FIG. 3. (Color online) Phase diagrams for values of $\alpha = \Delta_1/\Delta_2$, with Chern number for each phase. The dots in panel (b) indicate values of $t_1/\mu, t_2/\mu$ investigated numerically.

The hybridization effects also depend on the bulk parameters of the system, i.e., t_1, t_2, Δ_1, Δ_2, and μ. In particular, as these parameters are tuned to the phase transitions, the edge-vortex length scale diverges. Such tuning is explored in a system with $(\Delta_1, \Delta_2) = (0.5, 1.0)$ and $t_1 = -2$ (energy is

given in terms of the NNN hopping strength, t_2) by adjusting the chemical potential μ, i.e., by moving along the path shown in Fig. 3, which crosses several phase transitions. In the Chern number 3 portion of the phase diagram, we find that the spatial period of vortex-vortex oscillation increases linearly with the chemical potential: $\Lambda \sim 0.8\mu + \text{constant}$. When μ takes on values putting the system too close to the phase transition, edge-vortex hybridization destroys the vortex-vortex oscillatory behavior.

Another issue addressed in the numerical simulation is the number of low-energy modes created around defects. When only NNN interactions are present, one Majorana mode per vortex per sublattice forms. When the NN terms are turned on, the Majoranas may hybridize down to zero or one residual zero-energy mode, for even and odd Chern number, respectively.[15] Interestingly, there is some degree of protection of the additional defect mode for the Chern number 2 phase. The numerical simulation reveals two, apparently disorder-resistant, zero-energy vortex-core modes. The Chern number 3 phase, however, enjoys no such additional modes: only one low-energy vortex-core mode is observed in the numerical simulations.

Having introduced the primary results of the paper, the remainder of the paper explains details of our approach. First, in Sec. II, we describe the Hamiltonian used (including both nearest- and next-nearest-neighbor terms) and calculate its Chern number analytically. Next, in Sec. III, we describe the defects added to our model Hamiltonian: edges, disorder, and magnetic fields. Finally, in Sec. IV, we discuss the numerical attack on the system, with defects present, and the resulting conclusions. Additional details are in the appendices: a brief review of the calculation of Chern numbers (Appendix A), and a discussion of a spatial inversion symmetry of the system helpful in distinguishing different modes (Appendix B).

II. NOTATION AND DEFECT-FREE ANALYSIS

A. System definition

Here, we describe the model system: a single-band, two-dimensional, tight-binding, spinless fermion square lattice model with mean-field superconducting order parameter Δ, and Hamiltonian

$$
\begin{aligned}
H &= \sum_{ij} h_{ij} c_i^\dagger c_j + \frac{1}{2} \sum_{ij} \Delta_{ij} c_i^\dagger c_j^\dagger + \text{H.c.} \\
&= \frac{1}{2} \sum_{ij} [c_i^\dagger \quad c_i] \begin{bmatrix} h_{ij} & \Delta_{ij} \\ \bar{\Delta}_{ji} & -\bar{h}_{ij} \end{bmatrix} \begin{bmatrix} c_j \\ c_j^\dagger \end{bmatrix} \\
&= \frac{1}{2} \sum_{ij} [c_i^\dagger \quad c_i] \mathcal{H}_{ij} \begin{bmatrix} c_j \\ c_j^\dagger \end{bmatrix} = E_g + \sum_n E_n \Psi_n^\dagger \Psi_n, \quad (1)
\end{aligned}
$$

where the indices i and j run over all lattice sites. The lattice separation a is set to unity. The Bogoliubov–de Gennes Hamiltonian is diagonalized in the last step in terms of the ground-state energy E_g, quasiparticle energies E_n, and operators

$$
\Psi_n = \sum_i \left[u_i^{(n)} c_i + v_i^{(n)} c_i^\dagger \right]. \quad (2)
$$

The hopping and pairing terms are stated here explicitly and illustrated in Fig. 2. The lattice separation is set to 1, and j runs over all lattice sites:

$$
h_{j,j} = O_j - \mu, \quad (3)
$$

$$
h_{j,j\pm\hat{x}} = h_{j,j\pm\hat{y}} = t_1, \quad (4)
$$

$$
h_{j,j\pm(\hat{x}+\hat{y})} = h_{j,j\pm(\hat{x}-\hat{y})} = t_2, \quad (5)
$$

and

$$
\Delta_{j,j\pm\hat{x}} = \pm i\Delta_1 \quad \text{and} \quad \Delta_{j,j\pm\hat{y}} = \pm \Delta_1, \quad (6)
$$

$$
h_{j,j\pm(\hat{x}-\hat{y})} = \pm i\Delta_2 \quad \text{and} \quad h_{j,j\pm(\hat{x}+\hat{y})} = \pm \Delta_2, \quad (7)
$$

with all other terms zero. The on-site term is separated into the chemical potential μ, and all other on-site terms O_j, such as disorder and edges.

For both the NN and NNN pairing terms, the phase of the order parameter advances under counterclockwise rotation, creating the chirality of the order parameter.[27] The pairing terms explicitly break time-reversal symmetry, putting the two dimensional system in Altland-Zirnbauer[23] symmetry class D, with topological classification $\mathbb{Z}$ given by the Chern number.[19] Indeed, we will show that the system takes on Chern numbers -3 through 3 in the following three subsections.

B. Gap closing momenta and symmetries

In this section, we follow a well-known program for calculating Chern numbers; a brief review is provided in Appendix A. After Fourier-transforming the Hamiltonian (1), the bulk band gap is seen to collapse for momenta $\boldsymbol{k} = (k_x, k_y)$ such that

$$
\begin{aligned}
0 = \frac{1}{2\Delta_2} \Delta(k) &= \alpha[\sin(k_x) + i \sin(k_y)] \\
&+ \sin(k_x - k_y) + i \sin(k_x + k_y) \quad (8)
\end{aligned}
$$

and

$$
\begin{aligned}
0 = \frac{1}{\mu} h(k) &= -1 + 2\left(\frac{t_1}{\mu}\right)[\cos(k_x) + \cos(k_y)] \\
&+ 4\left(\frac{t_2}{\mu}\right)\cos(k_x)\cos(k_y). \quad (9)
\end{aligned}
$$

Our procedure identifies the zeros of $\Delta(\boldsymbol{k})$ and then characterizes $h(\boldsymbol{k})$ at these momenta.

C. Zeros of Δ

There are the four zeros of Δ at the high-symmetry points (i.e., where $\sin k_x = \sin k_y = 0$). Assuming that the sine terms do not vanish, the remaining four zeros of Δ can be shown to satisfy

$$
\begin{aligned}
\cot(k_x)^2 &= \frac{\alpha^2}{2 - \alpha^2}\left[1 + \sqrt{\frac{4}{4 + \alpha^4}}\right], \\
\cot(k_y)^2 &= \frac{\alpha^2}{2 - \alpha^2}\left[1 - \sqrt{\frac{4}{4 + \alpha^4}}\right].
\end{aligned} \quad (10)
$$

Thus, there are two cases: $\alpha^2 \geqslant 2$, in which $\Delta(\boldsymbol{k})$ only vanishes at the four high-symmetry points, and $\alpha^2 < 2$, for which
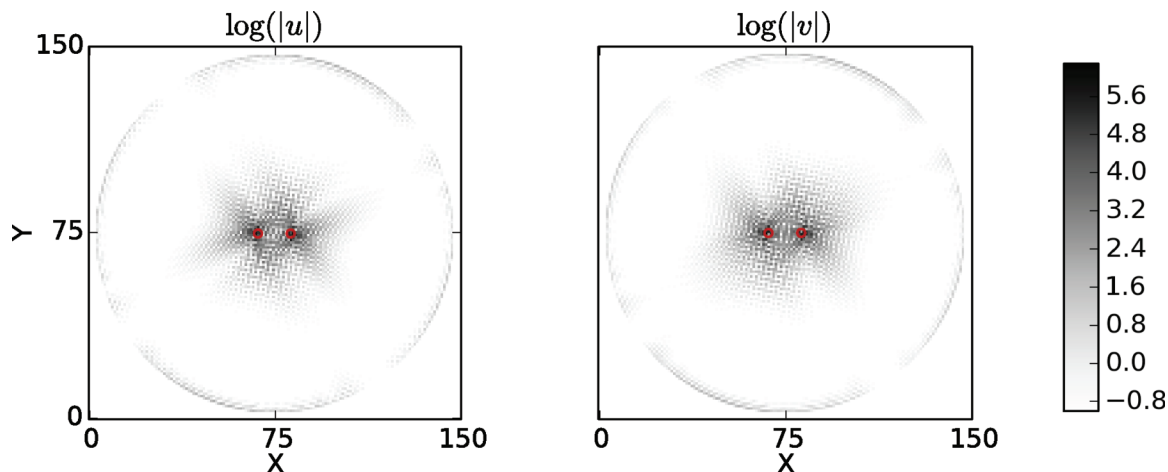
FIG. 4. (Color online) Plot of the wave function of a vortex mode. The lattice is 150×150, $t_1 = -2$, $\mu = 1$, and $(\Delta_1, \Delta_2) = (0.5, 1.0)$ (energy given in units of t_2). The plots are of the natural logarithm of the probability densities of the $\begin{bmatrix} u \\ v \end{bmatrix}$ parts of the BdG wave function. The Hamiltonian includes two vortices of radius $r_V = 1.6$ indicated by red circles, separated by 13.2 in the x direction. The eigenenergy is in-gap: $E/t_2 \approx 5.3 \times 10^{-3}$.

the order parameter vanishes at two additional, α-dependent momenta. A straightforward, if lengthy, consideration of cases of the signs of the $\cos(k_i)$ and $\sin(k_i)$ would allow the cotangent terms to be plotted implicitly, giving an exact solution for the location in the Brillouin zone for each zero. Fortunately, an explicit solution for the momenta of the zeros is not needed, as we will see momentarily.

D. h at the zeros of Δ

For $\boldsymbol{k}$ such that $\Delta(\boldsymbol{k}) = 0$, the band gap closes if and only if $h(\boldsymbol{k}) = 0$. Furthermore, the phase winding of Δ around its zeros and the sign of $h(\boldsymbol{k})$ at each zero indicate the Chern number. This well-known result is reviewed in Appendix A. At the high-symmetry points Γ, X, Y, and M,

$$\frac{1}{4\mu} \begin{bmatrix} h(0,0) \\ h(\pm\pi,0) \\ h(0,\pm\pi) \\ h(\pm\pi,\pm\pi) \end{bmatrix} = \begin{bmatrix} t_2/\mu + t_1/\mu - \frac{1}{4} \\ -t_2/\mu - \frac{1}{4} \\ -t_2/\mu - \frac{1}{4} \\ t_2/\mu - t_1/\mu - \frac{1}{4} \end{bmatrix}. \quad (11)$$

By setting $h(\boldsymbol{k}) = 0$, we get the three α-independent phase transition lines: $t_2/\mu = -1/4$, $t_2/\mu + t_1/\mu = 1/4$, and $t_2/\mu - t_1/\mu = 1/4$. The Chern number changes by 1 when crossing each line (except for the $t_1/\mu = -1/4$ double line, where the change is 2). At the α-dependent zeros of Δ given by Eq. (10), h is evaluated (a tedious but straightforward considerations of cases):

$$\frac{1}{\mu} h(\boldsymbol{k}) = -1 - \left(\frac{t_1}{\mu}\right) \alpha(2 - \alpha^2) - \left(\frac{t_2}{\mu}\right) \alpha^4. \quad (12)$$

The condition that the α-dependent zeros are included or excluded by the Fermi surface [i.e., $h(\boldsymbol{k}) \lessgtr 0$] is recast by defining

$$\boldsymbol{\beta} = \begin{bmatrix} -\alpha(2 - \alpha^2) \\ -\alpha^4 \end{bmatrix} \quad \text{and} \quad \boldsymbol{t} = \frac{1}{\mu} \begin{bmatrix} t_1 \\ t_2 \end{bmatrix}, \quad (13)$$
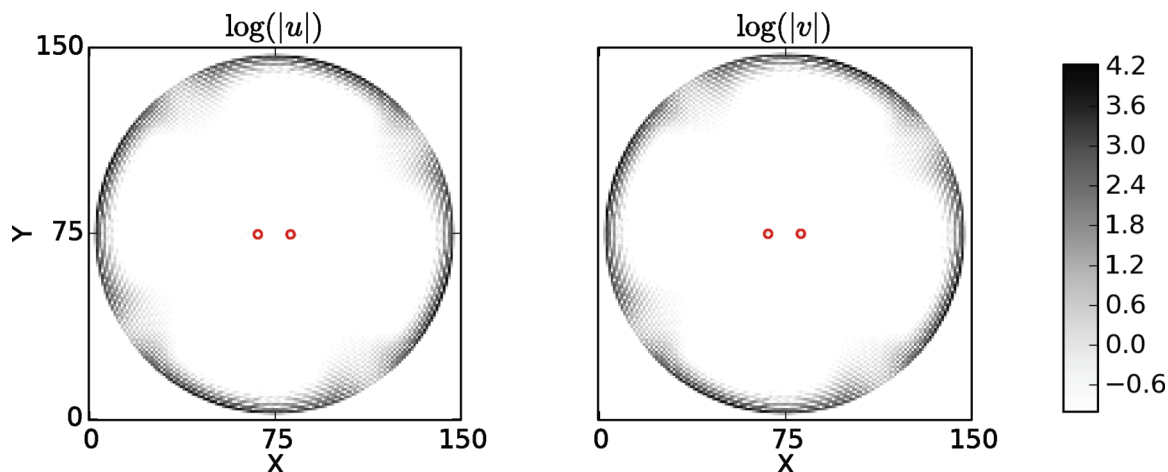

FIG. 5. (Color online) Plot of the wave function of an edge mode; compare with Fig. 4. The eigenenergy is in-gap: $E/t_2 \approx 3.1 \times 10^{-3}$. The state hybridized weakly with the vortices.

and the above condition can be restated as

$$0 \leqslant \frac{1}{\mu} h(\boldsymbol{k}) = -1 + \boldsymbol{t} \cdot \boldsymbol{\beta} \quad \text{or} \quad \frac{1}{\beta} \leqslant \boldsymbol{t} \cdot \hat{\boldsymbol{\beta}}; \quad (14)$$

i.e., there is a phase transition line, with closest approach to the t_1-t_2 origin given by $Z = \frac{\hat{\beta}}{\beta}$. Plotting these four phase transition lines, identifying the topologically trivial phase where where $(t_1, t_2) = (0, 0)$, and counting the number of lines crossed allows for the creation of phase diagrams for various values of α, such as those in Fig. 3.

III. DEFECTS AND MAGNETIC FIELDS

A. Magnetic fields: flux tubes and vortices

Here, we explore the response of the superconductor to magnetic fields. We assume we are in an extreme type-II limit: flux tubes form creating real-space vortices in the superconducting order parameter. In the two dimensional case at hand, the associated response currents are essentially two dimensional and therefore very weak. The natural simplifying limit is to take the London penetration depth $\lambda \to \infty$ and neglect the response magnetic field. We therefore assume a constant, unaffected, external magnetic field. Notwithstanding the infinite penetration depth, we still keep the superconducting coherence length ξ finite, allowing vortices in the superconducting order parameter. The vortices are therefore localized regions of vanishing superconducting order parameter Δ, without associated magnetic inhomogeneity, which we now describe more precisely.

We are guided by the relation

$$v_s = \frac{1}{2m} \left(\boldsymbol{\nabla}\phi - \frac{2e}{c} \boldsymbol{A} \right), \quad (15)$$

where v_s is the superfluid velocity, ϕ is the phase of the superconducting order parameter, and $\boldsymbol{A}$ is the vector potential, in London gauge. When far away from a vortex ($r \gg \lambda$), we assume $v_s = 0$ and $\boldsymbol{B} = 0$. Integrating around the vortex yields

$$2\pi n = \oint \boldsymbol{\nabla}\phi \cdot d\boldsymbol{l} = \frac{2e}{c} \Phi_m$$

(i.e., the well-known fact that an integer multiple of magnetic flux quanta penetrates through a flux tube). Because the order parameter is nonzero away from vortices, even for $r < \lambda$, the winding is an integer multiple of 2π around each vortex.

With a qualitative description of the behavior of the order parameter (the magnitude falls off near vortices, and the phase winds an integer multiple of 2π around each vortex), a quantitative model to perform a numerical simulation must now be established. We use the model[24,25]

$$\Delta_{jk} = \Delta_{k-j}^{(0)} \mathcal{D}(j,k) e^{i\theta_{jk}}. \quad (16)$$

The phase of the order parameter θ_{jk} is a geometric mean of the expected phases at j and k:

$$e^{i\theta_{jk}} = \frac{e^{i\phi_k} + e^{i\phi_j}}{|e^{i\phi_k} + e^{i\phi_j}|}. \quad (17)$$

(The arithmetic mean of ϕ_i and ϕ_j is insufficient, because the phase for pairing terms crossing any branch cut would be

incorrect.) Near the vortex cores, $\mathcal{D}$ falls off as

$$\mathcal{D}(j,k) = \frac{d_{\text{eff}}(j,k)}{\sqrt{d_{\text{eff}}(j,k)^2 + r_V^2}}, \quad (18)$$

where the "effective distance" is given by

$$d_{\text{eff}}^{-1}(j,k) = \sum_n \left(\min_{x \text{ between } j \text{ and } k} |x - v_n| \right)^{-1}; \quad (19)$$

x lies on the line connecting j and k. The vortex core radius r_V is a parameter of the model, on the order of the superconducting coherence length. Provided that vortices were separated from each other and the edge by many multiples of r_V, the vortex core size was to only weakly affect the measured properties of the system. To reduce the required lattice sizes for numerical stability, we set $r_V = 1.6$, the same order of magnitude as the coherence length in the cuprates. The hopping terms h_{jk} acquire a Peierls phase due to the magnetic vector potential

$$h_{jk} = h_{k-j}^{(0)} e^{i\frac{e}{c}\int_k^j \boldsymbol{A} \cdot d\boldsymbol{\ell}}.$$

Relation (15) expresses $\boldsymbol{A}$ in London gauge: $\boldsymbol{\nabla} \cdot \boldsymbol{A} = 0$ and the normal component of $\boldsymbol{A} \cdot \hat{n}$ becomes the physically meaningful boundary supercurrent. By choosing a gauge where $\boldsymbol{A}$ vanishes at the center of the sample, the vector potential for a constant magnetic field takes the simple form $\boldsymbol{A} \propto \rho\hat{\phi}$, where ρ is the distance from the center of the sample. Additionally, for our choice of $\boldsymbol{A}$, the boundary current vanishes for circular geometry. For noncircular geometries, the approximation will remain valid provided that the edge (and associated currents) is far from the features of interest.

B. Edges

Square edges can be produced by omitting certain terms in the Hamiltonian, i.e., setting all terms of the form h_{ij} and Δ_{ij} to zero for ij which cross an edge. While intuitive and simple, when two edges are introduced, an artificially "sharp" corner is produced. The low-energy edge modes that develop are strongly concentrated at the artificial corners. One might be concerned that such an unphysical feature might poison the simulation.

A choice of smoother edge removes the unphysically sharp corners, but introduces another problem: there are now lattice sites "outside" of the region of interest. The spectrum will include the unphysical quasiparticle modes outside the edge, complicating the analysis. A more natural approach is to make occupation of states beyond the edge energetically unfavorable. On-site terms $O_i c_i^\dagger c_i$ are added with O_i increasingly large near and beyond the edges of the system. For our purposes, the edge is made very steep and circular; i.e., it goes from 0 inside a circular region of the lattice to a very large number outside it. The lattice sites with large on-site energies must play no role in the low-energy spectrum of the Hamiltonian.

C. Disorder

By adjusting the O_i terms, on site disorder is produced, representing quenched impurities on the lattice. The model is

$$O_i = \begin{cases} 0, & \text{with probability } 1 - p, \\ -E_d, & \text{with probability } p/2, \\ +E_d, & \text{with probability } p/2. \end{cases}$$

When vortices are moved, such as in Fig. 9, the same disorder realization is used for each vortex placement.

IV. NUMERICAL RESULTS

Here, we discuss the results of the numerical diagonalization of the Bogoliubov–de Gennes Hamiltonian (1) for eigenvalues near zero. These midgap states arise because of the topological nature of the system. Being deep inside the superconducting gap, these midgap states experience strong particle-hole mixing. As lattice sizes and vortex separation are increased, hybridization dies off, quasiparticle energies go to zero, and the particle and hole parts can be made equal, $|u| = |v|$. In our realistic case of finite separation, there will always be nonzero hybridization, and consequential deviation from equality.

We put $(\Delta_1, \Delta_2) = (0.5, 1.0)$, and always work with energy in units of the NNN hopping, t_2. Our choice of parameters creates a rich phase diagram while keeping the magnitudes of both NN and NNN pairing terms similar. Several choices of t_1/t_2 were investigated, but all focus on exploring $t_1 < 0$ and $t_2 > 0$, which is similar to the superconducting band of the strontium ruthenates.

The output of the numerical simulation is the low-energy spectrum and associated wave functions. Both vortex core states, such as Fig. 4, and edge states, such as Fig. 5, are part of the output. Although presented as distinct in the examples, they can and do hybridize. To distinguish the edge and vortex
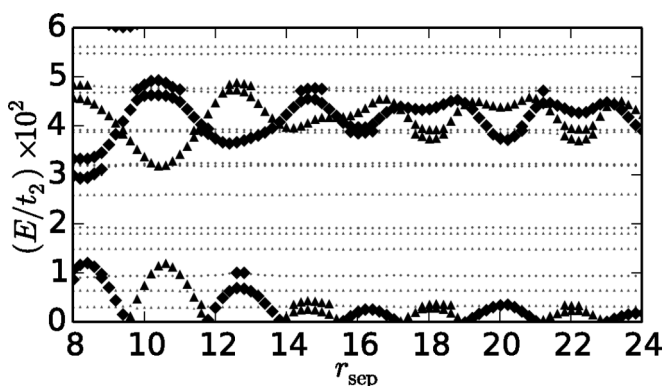

FIG. 6. Plot of several lowest quasiparticle energies as the separation between two vortices in the x direction is varied. The lattice was 150×150, with a circular edge. The other parameters are $(\Delta_1, \Delta_2) = (0.5, 1.0)$, $\mu = 1$, and $t_1 = -2.0$ (energies are given in terms of t_2). The choice of parameters leads to Chern number 3 and a single zero-energy vortex core mode, as guaranteed for odd Chern numbers; cf. Fig. 7. The shapes of the markers indicate the parity of the state under spatial-inversion symmetry: diamond is even, and triangle is odd (see Appendix B). The unimportant edge states are indicated by the smaller, fainter markers.
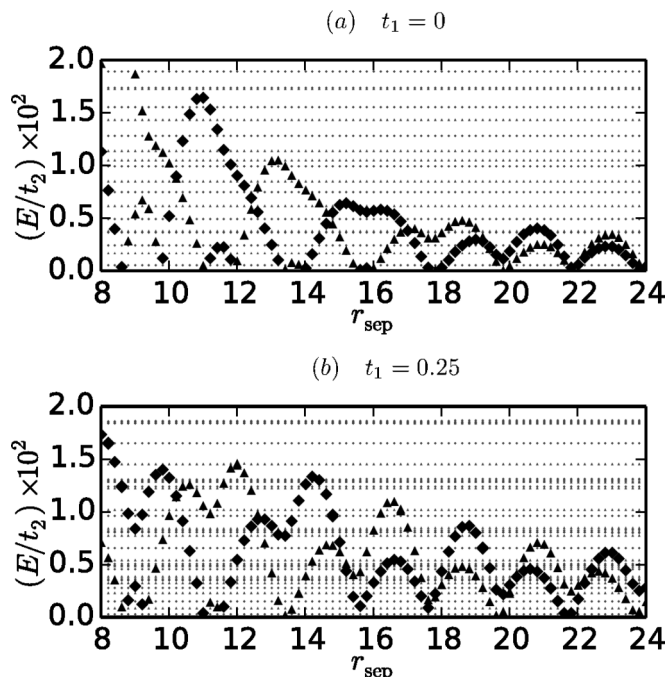

FIG. 7. Compare with Fig. 6: circular lattice, $(\Delta_1, \Delta_2) = (0.25, 0.5)$, and the chemical potential $\mu = 0.5$. Each panel has a different value of t_1, as shown; all energies are given in terms of t_2. The vortex separation r_{sep} is given in terms of lattice spacing. Notice the *two* oscillating low-energy excitations, possibly with an exponentially damped envelope. In the limit of large separation of the vortices, these vortex core states could become 0-energy Majorana modes. We suspect that that a significant portion of the Chern number -2 phase enjoys these multiple Majorana modes, suggesting analytical investigation. Resistance to weak disorder is discussed later, Fig. 9.

states automatically, the probability of a state being present within some distance of the edge is found and used to classify a given state as "edge" or not. As seen in, for example, Fig. 6 with $r_{\text{sep}} \approx 13$, the edge-vortex hybridization becomes strong enough to cause the third edge modes to hybridize strongly
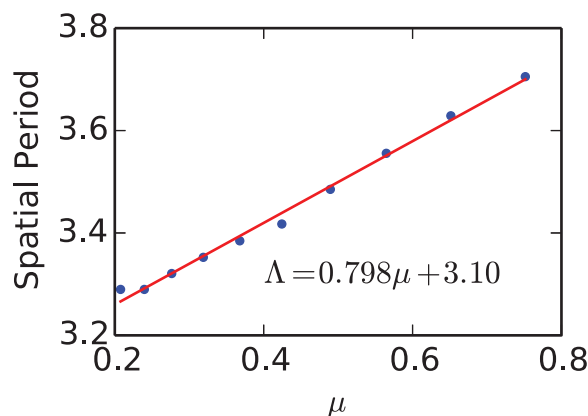

FIG. 8. (Color online) Spatial period of oscillation of vortex mode energy as two vortices are separated in the x direction, as in Fig. 6. The spatial period changes as the chemical potential μ is varied (all other parameters are as in the aforementioned figure). For plotted values of μ, the Chern number was 3. Larger values of μ were inaccessible due to edge-vortex hybridization.

with the vortex modes, resulting in significant occupation away from the edge. In general, however, edge modes, being localized away from the vortices (due to the careful choice of parameters), do not strongly influence the low-energy vortex core modes.

A. Vortex core mode oscillations

When the separation between two magnetic vortices is adjusted, the spectrum shifts, as seen in Fig. 6 and Fig. 7. Most notably, the energies of the lowest quasiparticles exhibit damped oscillation. The dominant Fourier component of these oscillations is found (and inverted) to give a spatial period. The spatial period Λ is found as a function of the chemical potential μ in Fig. 8 for $t_1 = -2$, $\Delta_1 = 0.5$ (energy given in terms of t_2). The only values of μ shown are where the vortex core mode only hybridized weakly with the edge modes. Even small distortions to the oscillations disturb the calculation of the spatial period significantly. Systems close to criticality were therefore not examined. In particular, only points in the Chern number 3 phase were far enough from criticality to be calculated reliably. In that region, Λ was found to depend linearly on μ, with slope close to 0.8. As mentioned before, these oscillations have been analytically[21] and numerically[22] investigated before (for slightly different systems) with a period $\sim \frac{2\pi}{k_F}$, due to the oscillations in the vortex mode wave functions on the same spatial period.

B. Majorana mode count

For Chern number 3, only one vortex mode exists; see Fig. 6. However, for Chern number ± 2, two 0-energy modes develop when two vortices are introduced. Modes in the -2 region near $t_1 = 0$ are examined in Fig. 7. The Chern number $+2$ region [with, e.g., $(t_1/\mu, t_2/\mu) = (-1.5, 2)$ in Fig. 3] probably also supports an additional vortex mode, but the issue there is complicated by the fact that the system is usually quite close to criticality; i.e., the zeros of $\Delta(k)$ occur where h_k is relatively small, leading to a divergence of correlation lengths. Effective analysis requires that the edge-vortex hybridization be suppressed; much larger systems would have to be simulated.

C. Disorder

Here, we discuss the results on-site disorder to O_i mentioned earlier. The same simulations with disorder added are shown in Fig. 9. For weak disorder, pairs of vortex modes that exist without disorder persist after turning on the weak disorder. In reality, vortices would become pinned to disorder sites. A more detailed calculation would not install vortices at prespecified locations. Despite these caveats, we believe that these additional modes warrant further analytical investigation.

V. CONCLUSION

Chiral p-wave superconductors on a lattice support additional, interesting phases beyond the two well-known (topologically trivial) BEC and (Chern number 1) BCS phases. The Chern number ± 2 phases can be understood intuitively as a pair of weakly interacting sublattices: the defect modes

appear to survive variation of parameters as well as the addition of weak disorder. It is expected[15] that some perturbation of the Hamiltonian will hybridize the defect states, though the precise form of the interaction has not been determined. The Chern number 3 phase, on the other hand, does not support any additional modes. The consequences of including NNN interactions in two-dimensional chiral superconductors are worthy of analytical attention.

APPENDIX A: CHERN NUMBER REVIEW

Here, we review Chern number calculation in the defect-free case, as in Sec. II for nearest- and next-nearest interactions. In momentum space, the Hamiltonian (1) $\mathcal{H}_{ij}$ becomes $\mathcal{H}_k = \boldsymbol{n}_k \cdot \tau$, where τ is a vector of Pauli matrices and

$$\boldsymbol{n}_k = \begin{bmatrix} \Re \Delta_k \\ -\Im \Delta_k \\ h_k \end{bmatrix}. \qquad (A1)$$

The Chern number is obtained by integrating the Berry curvature

$$\frac{1}{2\pi} \boldsymbol{\nabla}_k \times \langle 0 | \Psi_k i \boldsymbol{\nabla}_k \Psi_k^\dagger | 0 \rangle = \frac{1}{4\pi} (\boldsymbol{\nabla}_k \Phi_k) \times (\boldsymbol{\nabla}_k n_k)$$
$$= \frac{1}{4\pi} \hat{\boldsymbol{n}} \cdot \frac{\partial \hat{\boldsymbol{n}}}{\partial k_x} \times \frac{\partial \hat{\boldsymbol{n}}}{\partial k_y} \qquad (A2)$$

over the Brillouin zone ($|0\rangle$ is the vacuum state). Both equalities are due to straightforward calculation. The vector-valued function $\boldsymbol{n}$ maps momentum space to $\mathbb{R}^3$, and characterizes the Cooper pairing (and corresponding quasiparticles) at a given momentum. The vanishing of $\boldsymbol{n}$ corresponds precisely to nodes in the band structure. Therefore, in the fully gapped regime, the unit vector $\hat{\boldsymbol{n}}$ maps T^2 to S^2, and the above integral is just the degree of the map $\hat{\boldsymbol{n}}$, an integer.[26] According to the Hopf classification, the degree characterizes the mapping $\hat{\boldsymbol{n}}$ topologically, i.e., up to homotopy. We emphasize here that we have so far said nothing about the presence of zero-energy modes or sublattices, only the topologically invariant Chern number.

One can do slightly better. By smoothly deforming $\boldsymbol{n}$ so that $\boldsymbol{n}$ is $\pm \hat{z}$ except when h_k vanishes, the Chern number is seen to depend only on the winding of the phase of the superconducting order parameter around the Fermi surface (of the parent state, i.e., where $h_k = 0$). Because such a smooth deformation will not close the band gap, the topological invariant is unchanged. The integral over the Brillouin zone therefore becomes a line integral over the $h_k = 0$ surface, which is sensitive only to the winding of the superconducting order parameter's phase ϕ.

The winding of ϕ can only occur around zeros of Δ, and always in multiples of 2π. Neglecting higher order zeros of Δ, one simply counts the number of zeros enclosed by the Fermi surface, and notes whether their winding is clockwise or counterclockwise to get the Chern number. To get the sign of the answer correct, "enclosed" is taken to mean the particle-like side of the Fermi surface. We emphasize now that we are dealing with a quadratic, *single-band* Hamiltonian. Analogous results for multiband Hamiltonians would be more complicated.

APPENDIX B: SPATIAL INVERSION SYMMETRY

In the absence of added disorder, the model systems we consider have a spatial inversion symmetry which can be exploited to enhance the clarity of some plots (especially in highlighting oscillatory behavior). The hopping terms straightforwardly satisfy $h_{-i,-j} = h_{ij}$, while the p-wave symmetry of the superconducting order parameter implies $\Delta_{-i,-j} = -\Delta_{ij}$.

Let $\mathcal{I}$ realize the inversion symmetry in position space [i.e., $(\mathcal{I}h)_{ij} = h_{-i,-j}$] and put $\mathscr{I} = \tau_3 \otimes \mathcal{I}$ (τ_3 acts on the space of Nambu spinors). Clearly, $\mathscr{I}^2 = 1$, and $\mathscr{I}^\dagger = \mathscr{I}$, so the eigenvalues of $\mathscr{I}$ are ± 1. The inversion symmetry's action on the Hamiltonian,

$$\mathscr{I}^\dagger \mathcal{H}_{ij} \mathscr{I} = \mathcal{I}^\dagger \tau_3^\dagger \mathcal{H}_{ij} \tau_3 \mathcal{I},$$

$$\mathcal{I}^\dagger \begin{bmatrix} h_{ij} & -\Delta_{ij} \\ -\bar{\Delta}_{ji} & -\bar{h}_{ij} \end{bmatrix} \mathcal{I} = \begin{bmatrix} h_{-i-j} & -\Delta_{-i-j} \\ -\bar{\Delta}_{-j-i} & -\bar{h}_{-i-j} \end{bmatrix}$$

$$= \begin{bmatrix} h_{ij} & \Delta_{ij} \\ \bar{\Delta}_{ji} & -h_{ij} \end{bmatrix} = \mathcal{H}_{ij}, \quad \text{(B1)}$$

shows that the inversion symmetry $\mathscr{I}$ relates quasiparticles of the form (u_i, v_i) to $(u_{-i}, -v_{-i})$. For appropriate energy eigenstates, $\psi = \pm \mathscr{I} \psi$ and the subparts u and v therefore have separate (and opposite) inversion symmetries given by $\mathcal{I}u = \pm u$ and $\mathcal{I}v = \mp v$. These eigenvalues can be changed using the Bogoliubov–de Gennes particle-hole symmetry
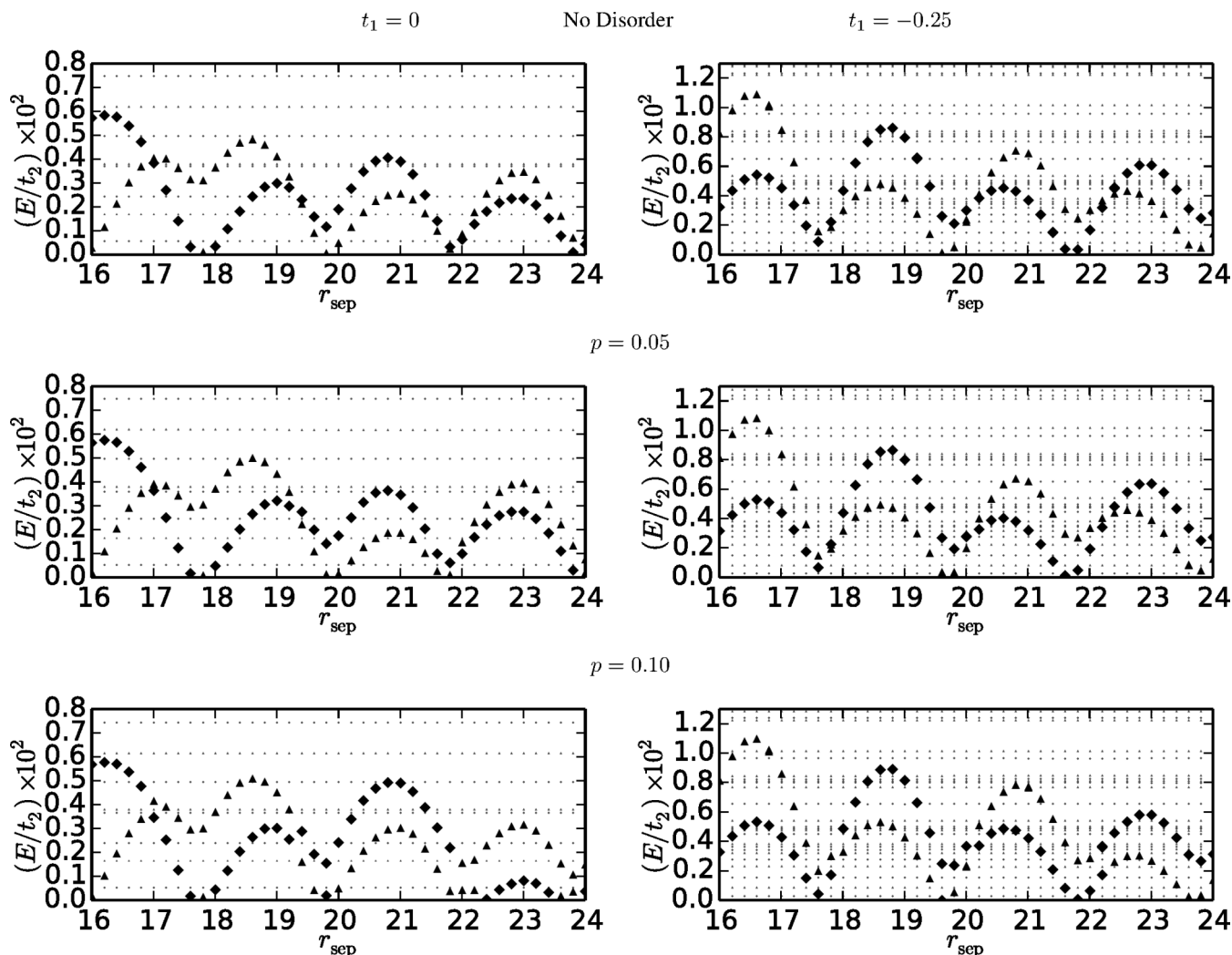

FIG. 9. Compare with Fig. 7; the choice of parameters is the same. The focus of these figures is on the disorder, of strength $E_d = \frac{1}{10}$ and probability p. All energies given in terms of t_2. Although disorder destroys inversion symmetry (discussed in Appendix B), there is still significant overlap of wave functions with their spatial inversion partner. The different markers indicate the sign of the overlap: positive is diamond, negative is triangle, and weak overlap is indicated by a circle. Weak disorder should not destroy exponentially damped oscillating behavior if it already exists; no qualitative changes occur when weak disorder is added.

(i.e., $\Xi = \tau_1 \otimes K$, where K is complex conjugation); the symmetry-related negative-energy pair has opposite $\mathscr{I}$ eigenvalue:

$$\Xi \mathscr{I} = \tau_1 K \tau_3 \mathscr{I} = -i \tau_2 \mathscr{I} = -\mathscr{I} \Xi. \tag{B2}$$

In the case of disorder, the symmetry $\mathscr{I}$ is clearly broken by the additional terms. Nonetheless, the overlap $\langle \psi | \mathscr{I} \psi \rangle$ is still meaningful: if positive, we can still identify ψ as "symmetric"-like or otherwise. In the figures, e.g., Fig. 9, the sign of the overlap is plotted as the shape of the symbol.

[1] V. Mourik, K. Zuo, S. M. Frolov, S. R. Plissard, E. P. A. M. Bakkers, and L. P. Kouwenhoven, Science **336**, 1003 (2012).

[2] A. Y. Kitaev, Phys. Usp. **44**, 131 (2001).

[3] F. Wilczek, Nat. Phys. **5**, 614 (2009).

[4] G. Moore and N. Read, Nucl. Phys. B **360**, 362 (1991).

[5] L. Fu and C. L. Kane, Phys. Rev. Lett. **100**, 096407 (2008).

[6] J. D. Sau, R. M. Lutchyn, S. Tewari, and S. Das Sarma, Phys. Rev. Lett. **104**, 040502 (2010).

[7] J. D. Sau, S. Tewari, R. M. Lutchyn, T. D. Stanescu, and S. Das Sarma, Phys. Rev. B **82**, 214509 (2010).

[8] J. Alicea, Y. Oreg, G. Refael, F. von Oppen, and M. P. A. Fisher, Nat. Phys. **7**, 412 (2011).

[9] J. Alicea, Phys. Rev. B **81**, 125318 (2010).

[10] R. M. Lutchyn, J. D. Sau, and S. Das Sarma, Phys. Rev. Lett. **105**, 077001 (2010).

[11] W. DeGottardi, D. Sen, and S. Vishveshwara, New J. Phys. **13**, 065028 (2011).

[12] J. Alicea, Rep. Prog. Phys. **75**, 076501 (2012).

[13] N. Read and D. Green, Phys. Rev. B **61**, 10267 (2000).

[14] D. A. Ivanov, Phys. Rev. Lett. **86**, 268 (2001).

[15] R. Roy, Phys. Rev. Lett. **105**, 186401 (2010).

[16] N. B. Kopnin and M. M. Salomaa, Phys. Rev. B **44**, 9667 (1991).

[17] G. Volovik, J. Exp. Theor. Phys. Lett. **70**, 609 (1999).

[18] C. Caroli, P. D. Gennes, and J. Matricon, Phys. Lett. **9**, 307 (1964).

[19] M. Z. Hasan and C. L. Kane, Rev. Mod. Phys. **82**, 3045 (2010).

[20] Y. Niu, S. B. Chung, C.-H. Hsu, I. Mandal, S. Raghu, and S. Chakravarty, Phys. Rev. B **85**, 035110 (2012).

[21] M. Cheng, R. M. Lutchyn, V. Galitski, and S. Das Sarma, Phys. Rev. Lett. **103**, 107001 (2009).

[22] T. Mizushima and K. Machida, Phys. Rev. A **82**, 023624 (2010).

[23] A. Altland and M. R. Zirnbauer, Phys. Rev. B **55**, 1142 (1997).

[24] A. Melikyan and Z. Tešanović, Phys. Rev. B **74**, 144501 (2006).

[25] O. Vafek and A. Melikyan, Phys. Rev. Lett. **96**, 167005 (2006).

[26] M. Nakahara, *Geometry, Topology, and Physics*, Graduate Student Series in Physics (IOP, Bristol, 2003).

[27] The case of opposite chirality, in which the NNN pairing has chirality opposite of the NN pairing, was investigated analytically. It is not included because it is not clear whether such terms are even physical. The results are surprisingly similar to the same chirality case: Chern numbers range from $+3$ to -3.